B. Yu
State Key Laboratory for Strength
and Vibration of Mechanical Structures,
School of Aerospace,
Xi'an Jiaotong University,
Xi'an Shaanxi 710049, P. R. China
e-mail: jo_elnino1987@163.com

B. Han
State Key Laboratory for Strength
and Vibration of Mechanical Structures,
School of Aerospace,
Xi'an Jiaotong University,
Xi'an Shaanxi 710049, P. R. China
e-mail: hanbinabc@stu.xjtu.edu.cn

C. Y. Ni
State Key Laboratory for Strength
and Vibration of Mechanical Structures,
School of Aerospace,
Xi'an Jiaotong University,
Xi'an Shaanxi 710049, P. R. China
e-mail: ncygz@126.com

Q. C. Zhang
State Key Laboratory for Strength
and Vibration of Mechanical Structures,
School of Aerospace,
Xi'an Jiaotong University,
Xi'an Shaanxi 710049, P. R. China
e-mail: zqc111999@mail.xjtu.edu.cn

C. Q. Chen
Department of Engineering Mechanics,
AML and CNMM,
Tsinghua University,
Beijing 100084, P. R. China
e-mail: chencq@tsinghua.edu.cn

T. J. Lu[1]
State Key Laboratory for Strength
and Vibration of Mechanical Structures,
School of Aerospace,
Xi'an Jiaotong University,
Xi'an Shaanxi 710049, P. R. China
e-mail: tjlu@mail.xjtu.edu.cn

Dynamic Crushing of All-Metallic Corrugated Panels Filled With Close-Celled Aluminum Foams

Under quasi-static uniaxial compression, inserting aluminum foams into the interstices of a metallic sandwich panel with corrugated core increased significantly both its peak crushing strength and energy absorption per unit mass. This beneficial effect diminished however if the foam relative density was relatively low or the compression velocity became sufficiently high. To provide insight into the varying role of aluminum foam filler with increasing compression velocity, the crushing response and collapse modes of all metallic corrugate-cored sandwich panels filled with close-celled aluminum foams were studied using the method of finite elements (FEs). The constraint that sandwich panels with and without foam filling had the same total weight was enforced. The effects of plastic hardening and strain rate sensitivity of the strut material as well as foam/strut interfacial debonding were quantified. Three collapse modes (quasi-static, transition, and shock modes) were identified, corresponding to different ranges of compression velocity. Strengthening due to foam insertion and inertial stabilization both acted to provide support for the struts against buckling. At relatively low compression velocities, the struts were mainly strengthened by the surrounding foam; at high compression velocities, inertia stabilization played a more dominant role than foam filling. [DOI: 10.1115/1.4028995]

Keywords: dynamic crushing, sandwich panel, corrugation, metal foam, finite element

1 Introduction

When a metallic sandwich panel with cellular core is subjected to static or dynamic uniaxial compression, it is important that the core possesses both high crushing strength and high energy absorption per unit mass. In other words, an idealized sandwich panel for energy absorption should exhibit a plateaulike stress versus strain curve so that it is able to absorb large amount of energy at a constant stress level [1]. For sandwich panels having corrugated cores, it has been envisioned that this may be achieved if proper lateral support to core members against plastic yielding and buckling is supplied. To this end, recently, Yan et al. [2] inserted high porosity aluminum foams having closed cells into the interstices of corrugated sandwich panels made of 304 stainless steel, as shown schematically in Fig. 1. A combined experimental and numerical study of the hybrid-cored sandwich was carried out under quasi-static compressive loading. It was demonstrated that the peak strength and energy absorption of the foam-filled panel were much greater than the sum of those of an empty corrugated panel and the aluminum foam alone. Subsequently, combining analytical modeling with FE simulation, Han et al. [3] investigated systematically the influence of key geometrical and material parameters upon the quasi-static compressive performance of aluminum foam-filled corrugated panels. The elastoplastic buckling wavelength of the core members was found to be significantly reduced and the transition from axial deformation to bending of the core member was much delayed, both of which contributing to the enhanced peak strength and energy adsorption of the foam-filled panel.

In addition to the work of Yan et al. [2] on aluminum foam-filled sandwiches with corrugated cores, Vaziri et al. [4] inserted

[1]Corresponding author.

Contributed by the Applied Mechanics Division of ASME for publication in the JOURNAL OF APPLIED MECHANICS. Manuscript received April 2, 2014; final manuscript received July 21, 2014; accepted manuscript posted November 6, 2014; published online November 21, 2014. Editor: Yonggang Huang.

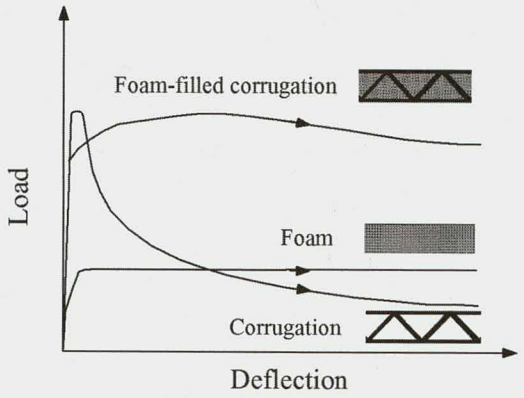

Fig. 1 Typical quasi-static compressive responses of empty corrugated panel, aluminum foam alone, and aluminum foam-filled corrugated panel

polymer foams (commercial name Divinycell) into the interstices of sandwich beams with either corrugated or honeycomb cores and investigated their performance with FE simulations. However, under either quasi-static or dynamic loading, as the lateral support provided by the relatively weak polymer foam to the core members was limited, the foam-filled sandwich beams showed no notable advantage over the corresponding empty sandwiches.

As a follow-up study of Yan et al. [2] and Vaziri et al. [4], this investigation aimed to characterize the dynamic compressive behavior of aluminum foam-filled sandwich panels as shown in Fig. 2(*a*) subjected to dynamic uniaxial crushing and impulsive loading. The influence of aluminum foam insertions on the peak stress and energy absorption of the hybrid-cored sandwich structures under varying compression velocities was quantified using FE simulations and the underlying physical mechanisms explored. In particular, the effectiveness of foam filling was assessed subjected to the constraint that corrugated panels with and without foam filler had the same total weight.

The paper was organized as follows. In Sec. 2, details of the FE model were described and relevant material properties specified. Section 3 presented the fundamental results of foam-filled corrugated panels under uniaxial dynamic compression, the effect of plastic hardening and strain rate sensitivity of the strut material was considered in Sec. 4. The influence of foam/strut interfacial bonding condition on the dynamic crushing of foam-filled panels

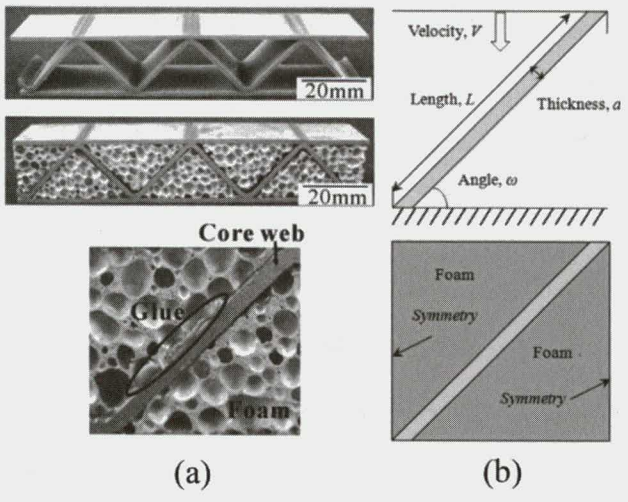

Fig. 2 (*a*) As-fabricated empty and foam-filled sandwich specimens and the interface between foam fillers and core web showing good bonding condition with epoxy glue and (*b*) specification of idealized FE model

was quantified in Sec. 5. In Sec. 6, as the compression velocity was increased, the roles of two mechanisms underlying the dynamic performance of the panel—foam strengthening and inertial stabilization—were discussed.

2 FE Modeling of Corrugated Sandwich Panels With Foam Insertions

2.1 FE Model. All the numerical calculations were performed using the FE code ABAQUS/EXPLICIT. The idealized FE model containing only one strut (i.e., core web) and the corresponding boundary conditions were shown schematically in Fig. 2(*b*). Let a and L denote separately the thickness and length of the strut. Unless otherwise stated, a was fixed at 1 mm a series of strut aspect ratios were considered (from $L/a = 20$ to $L/a = 60$), covering both relatively stocky struts and relatively slender struts. In the present paper, the inclination angle of the strut was fixed at $\omega = 45\text{deg}$.

The back face sheet of the panel was fixed, with no displacement or rotation allowed. A constant velocity V was imposed on the front face sheet so that the core was uniaxially compressed. In the case of the foam-filled panel, symmetry boundary condition was applied on the two side faces of the foam insertion; see Fig. 2(*b*). Both the front and back face sheets of the sandwich were assumed to be stiff enough to be modeled as rigid bodies. The strut was perfectly bonded to the front and back faces. Unless otherwise stated, the foam insertions, the face sheets as well as the struts were also perfectly bonded at the interface.

The strut and the foam insertions were both meshed using four-node plain strain quadrilateral elements with reduced integration (CPE4R in ABAQUS notation). Upon performing a mesh sensitivity study, an element size on the order of 0.05 mm (20 elements across the strut thickness) was shown to be sufficiently refined for ensuring the accuracy of the numerical results.

An initial deflection was introduced to the strut as the geometric imperfection. Unless otherwise stated, the form of the imperfection was chosen to be the same as the first buckling mode of the strut and the amplitude was taken as $0.03a$.

2.2 Material Properties. The strut material (304 stainless steel) was modeled as an isotropic and homogeneous elastic–plastic solid governed by von Mises yield criterion and J2 flow theory, with material parameters listed as follows: density $\rho_s = 8000\,\text{kg/m}^3$, Young's modulus $E_s = 200\,\text{GPa}$, Poisson ratio $\nu = 0.3$, and yield stress $\sigma_Y = 200\,\text{MPa}$. For plain strain conditions considered, $\bar{E}_s = E_s/(1-\nu^2) = 220\,\text{GPa}$ and $\bar{\sigma}_Y = 2\sigma_Y/\sqrt{3} = 231\,\text{MPa}$.

Both perfect plasticity (i.e., zero tangent modulus) and linear strain hardening for stainless steel were considered: for the latter a constant tangent modulus $E_t = 2\,\text{GPa}$ was employed; for plain strain, $\bar{E}_t = 4E_t/3 = 2.67\,\text{GPa}$.

Strain rate sensitivity was considered by

$$\sigma_D(\varepsilon_{pl}, \dot{\varepsilon}_{pl}) = R(\dot{\varepsilon}_{pl})\sigma_0(\varepsilon_{pl}) \tag{1}$$

where σ_D and σ_0 were, respectively, the dynamic and quasi-static yield stress, and R was a strain rate dependent multiplier. The dependence of R upon strain rate $\dot{\varepsilon}_{pl}$ was taken directly from the results of Stout and Follansbee [5].

The Deshpande and Fleck constitutive model [6] was adopted for the aluminum foams with closed cells. A series of foam relative densities, from $\bar{\rho}_f = 0.09$ to $\bar{\rho}_f = 0.19$, were employed to represent aluminum foams with relatively high and low porosities, respectively. For aluminum foams having certain relative densities, the Young's modulus E_P, the yield stress σ_P, and the strain hardening curve were calculated as functions of foam relative density according to a set of empirical formulas experimentally validated by Hanssen et al. [7], representing a set of reasonable parameters in reality.

$$E_p = 330\bar{\rho}_f^{2.45}(\text{GPa}) \quad (2)$$

$$\sigma_p = 720\bar{\rho}_f^{2.33}(\text{MPa}) \quad (3)$$

The Poisson ratio of the aluminum foam was fixed at 0.3. The densification strain was assumed to be $\varepsilon_D = 1 - 1.4\bar{\rho}_f$ [8].

For two reasons, the strain rate sensitivity of aluminum foam was not considered in the present study: first, under high compression velocities, the influence of strain rate sensitivity was much smaller compared to that of strengthening caused by shock wave propagation [9]; second, whether aluminum foam exhibited significant strain rate sensitivity remained an open issue, especially when the foam relative density was relatively small (less than ~0.2).

3 Dynamic Crushing Response

In this section, the strut material was modeled by an elastic–perfect plastic, rate independent constitutive model combined with the von Mises yield criterion and the J2 flow theory. The effect of strain hardening and rate sensitivity was considered later in Sec. 4.

3.1 Collapse Modes. Following McShane et al. [10], the core compression rate was expressed by dimensionless front face sheet velocity $\bar{V} = V/(c_{pl}\sin\omega)$, where $c_{pl} = \sqrt{\bar{\sigma}_Y/\rho_s}$ stood for the plastic wave speed in a nonhardening solid. The FE simulations presented below covered the velocity range of $\bar{V} = 0.0083 - 1.7$, equivalent to $V = 1 - 200\,\text{m/s}$. With focus placed upon the early stage of deformation and the contribution due to strut/foam interaction, the core was compressed up to a strain of $\varepsilon = 0.3$. Various foam relative densities (from $\bar{\rho}_f = 0.09$ to $\bar{\rho}_f = 0.19$) and strut aspect ratios (from $L/a = 20$ to $L/a = 60$) were considered, yielding different types of core configuration.

For selected compression velocities, Fig. 3 presented the histories of face sheet reaction force F as well as the deformation patterns, with $L/a = 20$ and $\bar{\rho}_f = 0.19$; contours of the equivalent plastic strain field were also shown in the snapshots of the deformation pattern. Other core types exhibited somewhat similar characteristics and hence were not shown here for brevity. Here, F denoted the normal component of the reaction force for a single unit cell per unit length, and $F_Y = \sigma_P L\cos\omega + \bar{\sigma}_Y a\sin\omega$ was the quasi-static reaction force when both the strut and foam insertions yield. To investigate the influence of foam relative density, Fig. 4 presented the front face reaction force histories and strut deflection profiles at $\varepsilon = 0.3$ for both empty and foam-filled panels, with $L/a = 20$.

As the compression velocity was increased, three different collapse modes of the foam-filled corrugated core may be identified from the results shown in Figs. 3 and 4, as follows:

(1) *Quasi-static mode*. When the compression velocity was sufficiently low, the stress wave propagation speed was much larger than the compression velocity. The core quickly reached equilibrium and, therefore, the reaction forces on the front and back face sheets were always equal. The buckling mode of the strut was similar to the case of quasi-static compression, with plastic hinges distributed irregularly along the strut and reduced buckling wavelength compared to the case of empty panel.

Figure 3(*a*) presented the reaction force history and deformation pattern of a foam-filled panel with $L/a = 20$ and $\bar{\rho}_f = 0.19$ at $\bar{V} = 0.0083$ (equivalent to $V_0 = 1\,\text{m/s}$). The reaction forces acting on the front and back faces were not distinguishable as mentioned above. At about $F/F_Y = 1$, the core (including the strut and the foam insertion) entered the plastic deformation regime and the reaction force remained constant. From the equivalent strain field contour, it was seen that the foam was highly strained around the plastic hinges, it remained almost undeformed near the undeflected portion of the strut. This indicated that the reaction force between the strut and the foam insertion was strongest where the strut was most deflected.

The compressive responses of foam-filled corrugated panels (with $\bar{\rho}_f = 0.09$ and $\bar{\rho}_f = 0.19$) as well as the empty corrugated panel were also compared in Fig. 4(*a*). The profiles of the strut central axis at $\varepsilon = 0.3$ for the three different core configurations were included as snapshots. Due to equilibrium through the core, only the reaction force on the front face sheet was plotted. The results of Fig. 4(*a*) demonstrated that plastic yielding was initiated in both empty and foam-filled panels at $F/F_Y = 1$. However, panels with different core configurations behaved rather differently beyond yielding. The empty panel (an inclined strut) experienced significant softening due to overall buckling (with wavelength equal to strut length L). In contrast, considerably reduced softening occurred in the foam-filled panel with $\bar{\rho}_f = 0.09$, no softening occurred and the reaction force remained nearly constant in the foam-filled panel with $\bar{\rho}_f = 0.19$. Clearly, the foam insertion provided strong lateral support to the strut against buckling, with

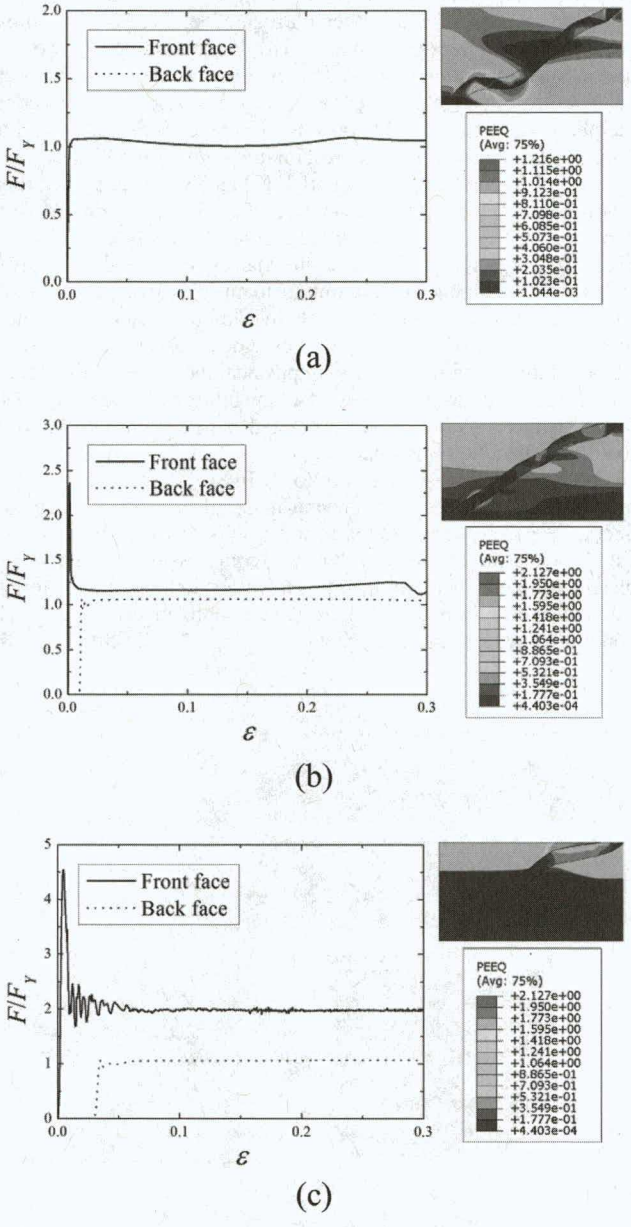

Fig. 3 Normalized reaction force on front and back faces and deformation patterns of foam-filled corrugated panel in terms of nominal compressive strain, $L/a = 20$ and $\bar{\rho}_f = 0.19$: (*a*) $\bar{V} = 0.0083$, (*b*) $\bar{V} = 0.33$, and (*c*) $\bar{V} = 1$

both the buckling wavelength and strut deflection reduced as the foam relative density was increased. The type II compressive behavior of empty panel was changed toward type I behavior by foam insertion, enabling more efficient energy absorption. This strengthening effect was negligible if the foam insertion was weak relative to the strut material as in the case of polymer foam [4].

(2) *Transition mode*. As the compression velocity was increased, the inertial effect became notable and its influence on the collapse behavior of the sandwich panel could no longer be neglected. In the presence of this inertial effect, the core was no longer in equilibrium as in the quasi-static case, causing a larger reaction force on the front face than that on the back face. Due to the so-called "buckle-wave" phenomenon [11], the buckling of the strut propagated together with the plastic wave along the strut and the buckling wavelength was considerably shorter than that of the quasi-static mode. Further, the deformation of the foam insertion was more concentrated toward the impact side compared to the quasi-static mode; see Fig. 3(*b*).

At the transition compression velocity of about $\bar{V} = 0.33$ (equivalent to $V = 40\,\mathrm{m/s}$), the reaction force on the back face of a foam-filled panel remained nearly constant at the yield load (i.e., $F/F_Y = 1$), for either $\bar{\rho}_f = 0.09$ or $\bar{\rho}_f = 0.19$ (results not shown for brevity). The reaction force on the front face also remained nearly constant after the initial peak (Fig. 3(*b*)), although slightly larger than that on the back face due to inertial effect. In contrast to the quasi-static case (Fig. 3(*a*)), the strut deflection was much smaller and the deformation in the foam was more concentrated toward the front face. Correspondingly, the largest equivalent plastic strain in the foam occurred around the strut end bonded to the front face. As the compression velocity was further increased, the tendency of the top portion of the strut to collide with the front face increased (Fig. 3(*b*)), causing the neighboring foam to be more compressed than elsewhere.

For the three core configurations considered (i.e., empty, $\bar{\rho}_f = 0.09$ and $\bar{\rho}_f = 0.19$), the normalized reaction force F/F_Y on the front face had almost the same value till the initial peak load was reached and diverged as the core was further compressed; see Fig. 4(*b*). The front face reaction force of the empty panel decreased while that of the foam-filled core exhibited no softening. However, in contrast to the quasi-static case (Fig. 4(*a*)), the softening of the empty panel at $\bar{V} = 0.33$ was milder as a result of inertial stabilization against lateral buckling due to the propagating buckle-wave. At about $\varepsilon = 0.25$, a second peak appeared due to hard contact between the significantly deformed strut (top portion nearly flat) and the moving front face; see Fig. 4(*b*). For a foam-filled panel, the propagating buckle-wave also reduced both the wavelength and amplitude of strut buckling. The strut deflection was further reduced by the constraint provided by the foam insertions, as justified by the strut deflection profiles shown in the snapshot. Again, a stronger foam led to smaller strut deflection although the strengthening effect was not as significant as in the quasi-static case. In summary, as the compression velocity was increased, the strut was increasingly stabilized by inertia, becoming much stronger relative to that compressed quasi-statically.

(3) *Shock mode*. When the compression velocity was high enough to generate shock wave in the foam, the deformation mode of the foam-filled panel considerably changed. Figures 3(*c*) and 4(*c*) presented the FE simulated results at the compression velocity of $\bar{V} = 1$ for corrugated panels ($L/a = 20$) having three different core configurations: empty, $\bar{\rho}_f = 0.09$ and $\bar{\rho}_f = 0.19$. The corresponding equivalent plastic strain in the foam shown in Fig. 5(*c*) for the case of $\bar{\rho}_f = 0.19$ exhibited a clear discontinuity, representing actually the propagating front of the shock wave. Further, no buckling occurred and the deformed strut was divided into two approximately straight portions linked by a plastic hinge;

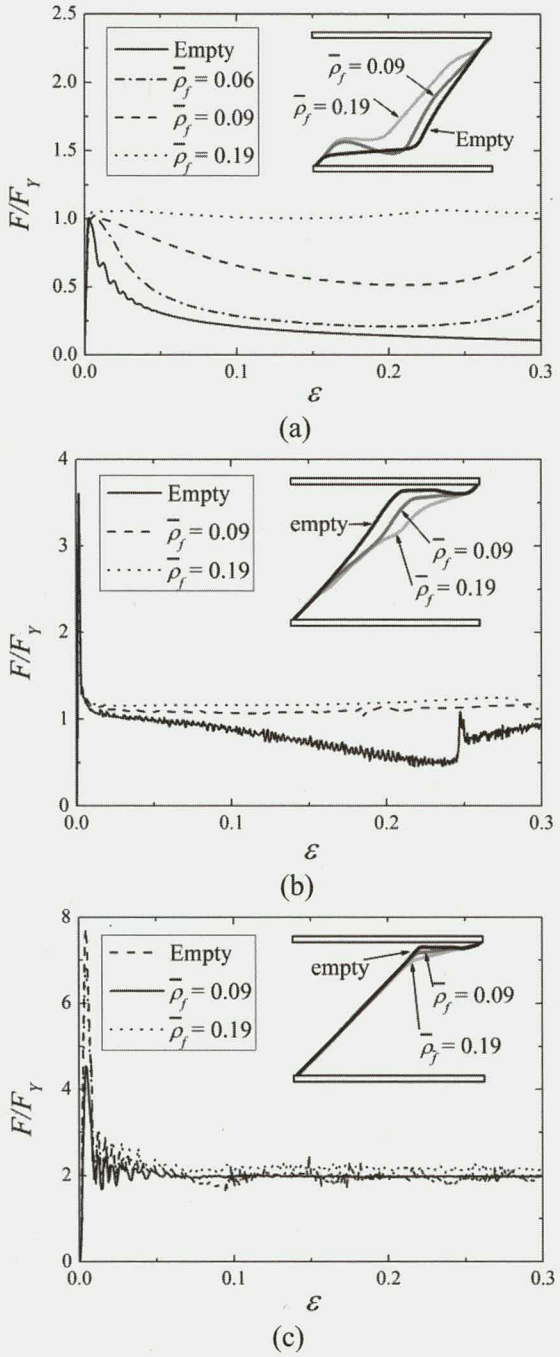

Fig. 4 Influence of foam relative density upon front face reaction force and strut deflection profile ($L/a = 20$): (*a*) $\bar{V} = 0.0083$, (*b*) $\bar{V} = 0.33$, and (*c*) $\bar{V} = 1$

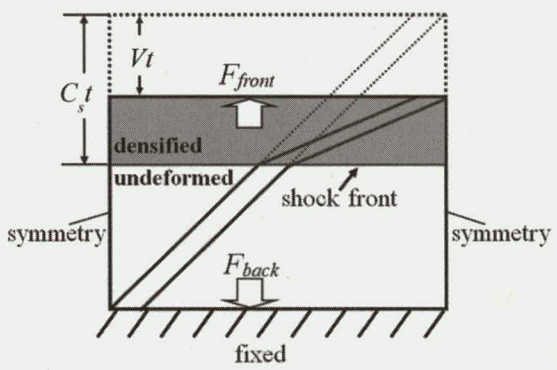

Fig. 5 Schematic representation of foam-filled corrugated core in shock regime. Dotted line denotes the initial configuration while solid line denotes the deformed one.

see snapshot of Fig. 3(*c*). The portion of the strut adjacent the front face was embedded in the densified layer of the foam and the stress in the densified layer was so elevated that the strut was not able to deflect.

The propagation of plastic wave was not exactly unidirectional because of the interaction between the strut and the inserted foam. Ahead of the shock front, the stress and equivalent plastic strain of the strut and the foam remained at the yield level and thus no deformation took place; see snapshot of Fig. 3(*c*). The plastic hinge traveled along the strut at approximately the same speed as the shock front propagating in the foam.

For the three core configurations considered (empty, $\bar{\rho}_f = 0.09$ and $\bar{\rho}_f = 0.19$), the reaction force on the front face exhibited little discrepancy (Fig. 4(*c*)) and was significantly larger than that on the back face, indicating strong inertial effect. This implied that the strengthening effect of the foam insertions as observed previously in the quasi-static and transition modes vanished.

3.2 Phenomenological Theoretical Description. Under quasi-static and transitional compression velocities, the strut buckling mode of the sandwich panels having different core configurations were significantly different. For compression velocities high enough to generate shock wave, however, the deformation pattern was nearly independent of foam relative density and strut slenderness, which was actually similar to that of a dynamically compressed inclined strut within the "stubbing" regime [10].

To analyze strut deformation within the "shock" regime, a schematic representation of the deformation pattern was presented in Fig. 5. It was assumed that the part of the foam-filled core behind the shock front (including the strut and the foam insertion) had attained the same velocity as the front face the rest of the core remained stationary. As no notable deformation was observed in front of the shock front in comparison with that in the shock-induced crushed region, agitation due to elastic wave propagation was neglected in modeling. Under these premises, the reaction force on the back face may be calculated as

$$F_{\text{back}} = \sigma_p L \cos\omega + \bar{\sigma}_Y a \sin\omega \tag{4}$$

By conservation of momentum, the reaction force on the front face became

$$F_{\text{front}} = F_{\text{back}} + \frac{d}{dt}[(\rho_f L \cos\omega + \rho_s a/\sin\omega) c_s t V] \tag{5}$$

where c_s was the propagating speed of the shock wave (Fig. 5). Given that $V = c_s \varepsilon_D$, the normalized form of the reaction forces may be expressed as

$$\frac{F_{\text{back}}}{F_Y} = 1 \tag{6}$$

$$\frac{F_{\text{front}}}{F_Y} = 1 + \frac{1}{\varepsilon_D}\left(\frac{\rho_f + \dfrac{2a\rho_s}{L\sin 2\omega}}{\sigma_p + \bar{\sigma}_Y \dfrac{a}{L}\tan\omega}\right) V^2 \tag{7}$$

3.3 Velocity Dependency of Normalized Average Reaction Force (NARF). The NARF was defined in order to reveal the important features of strut/foam interaction under different compression velocities, as

$$\bar{F} = \frac{\int_0^{\varepsilon} F d\xi}{\varepsilon F_Y} \tag{8}$$

Since the purpose of the present study was to characterize the early-stage dynamic crushing response of a foam-filled panel, the compressive strain in Eq. (8) was limited to $\varepsilon = 0.3$.

For quasi-static deformation, the NARF had a value smaller than 1, representing the loss of load capacity of the sandwich

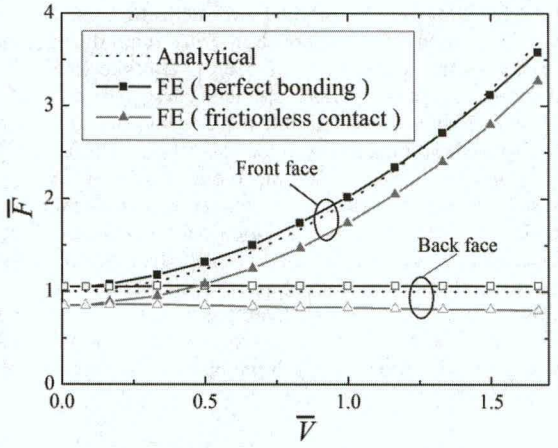

(a)

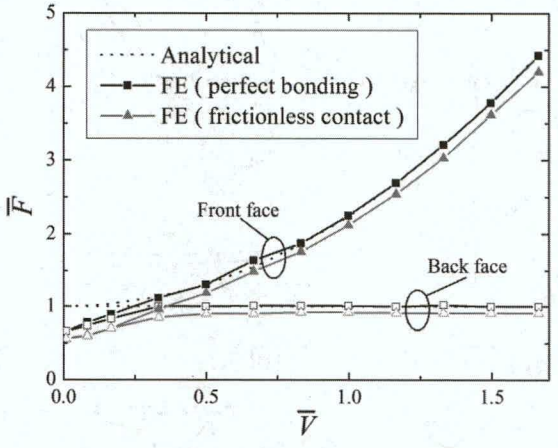

(b)

Fig. 6 NARF on face sheets of foam-filled corrugated panel plotted as a function of normalized compression velocity: (*a*) $L/a = 20$ and $\bar{\rho}_f = 0.19$ and (*b*) $L/a = 20$ and $\bar{\rho}_f = 0.09$

panel (either empty or foam-filled) due to elastic and/or plastic buckling of the strut. For transitional and shock deformation modes, the magnitude of the NARF was typically larger than 1, signifying the strengthening of the sandwich structure due to inertial stabilization effect as the compression velocity was increased.

Figures 6(*a*) and 6(*b*) plotted the numerically calculated $\bar{F}$ on both the front and back faces as a function of $\bar{V}$ for two core configurations ($\bar{\rho}_f = 0.09$ and $\bar{\rho}_f = 0.19$). Predictions with Eqs. (6) and (7) were also included for comparison. At low compression velocities such as $\bar{V} = 0 - 0.2$ (equivalent to $V = 0 - 24\,\text{m/s}$), the NARF on the front and back faces were equal. When $\bar{V} > 0.2$, the NARF on the front face diverged from that on the back face. As the compression velocity was increased, $\bar{F}_{\text{front}}$ exhibited a quadratic dependence on $\bar{V}$ while $\bar{F}_{\text{back}}$ was independent of the compression velocity, with $\bar{F}_{\text{back}} = \bar{F}_Y$.

For sandwiches filled with high relative density foams (e.g., $\bar{\rho}_f = 0.19$), the NARF $\bar{F}$ predicted using FE simulation agreed excellently well with the analytical prediction within the full range of compression velocity considered; see Fig. 6(*a*). For low foam relative densities, however, the NARF on both the front and back faces predicted by Eqs. (6) and (7) at low compression velocities were larger than those calculated numerically; see Fig. 6(*b*). This may be explained as follows: at low compression velocities, the foam fillers with a high relative density could provide constraint strong enough to stabilize the strut against lateral buckling, so that significant core softening was avoided and the reaction forces remained constant. In contrast, when the relatively density

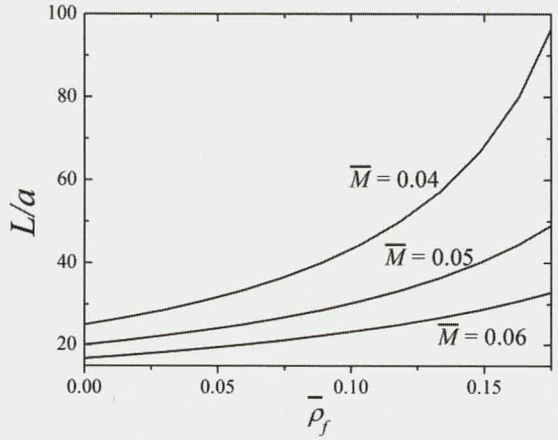

Fig. 7 Dependency of strut aspect ratio upon foam relative density

of the filling foam was small (i.e., the foam was mechanically weak), its stabilization effect was not sufficient to prevent core softening, reducing therefore the average reaction forces.

3.4 Constraint of Same Total Mass. The performance of a foam-filled sandwich structure was assessed below with the constraint that it had the same total mass as that of an empty sandwich [4]. To this end, instead of thinning the face sheets, the strut thickness was reduced as the foam relative density was increased. With the corrugation angle fixed at $\omega = 45$ deg, the normalized total mass of a unit cell of the foam-filled core may be expressed as

$$\bar{M} = \frac{M}{\rho_s L^2} = \frac{a}{L} + \frac{1}{2}\frac{\rho_f}{\rho_s} \tag{9}$$

For selected values of $\bar{M}$, the dependency of strut aspect ratio upon foam relative density was plotted in Fig. 7.

For the case where the total mass was fixed at $\bar{M} = 0.05$, the normalized reaction force versus strain curves for quasi-static mode, transition mode and shock mode were plotted in Figs. 8(*a*)–8(*c*), respectively; neither strain hardening nor rate sensitivity was considered and $\omega = 45$ deg. The corresponding deformation modes at $\varepsilon = 0.3$ for each case were inserted as snapshots. Compared to the case (Fig. 4) where the total mass was not constrained, no qualitative difference was observed.

From Fig. 8(*a*), it was seen that, under quasi-static loading, the foam-filled panel with a low foam relative density (e.g., $\bar{\rho}_f = 0.06$) exhibited a response similar to the empty panel. In other words, when the foam relative density is low, there is no clear advantage to filling the core with foam for structural purposes. This result is consistent with the findings of Vaziri et al. [4] for panels filled with weaker polymer foams. As the foam relative density was increased, however, the postbuckling strength of the foam-filled panel was strengthened and its reaction–strain curve became plateaulike when the foam relative density became sufficiently large, e.g., $\bar{\rho}_f = 0.19$. For the case of $\bar{\rho}_f = 0.09$, the second peak appearing in the response curve was attributed to the fact that the two plastic hinges shown in the snapshot were not formed simultaneously.

For either the transition mode or shock mode, the results of Figs. 8(*b*) and 8(*c*) revealed that the strut deformation was not significantly changed as the foam relative density was increased although the strut thickness was reduced as shown in Fig. 7.

4 Strain Hardening and Rate Sensitivity of Strut Material

To quantify the influence of strain hardening as well as rate sensitivity of the strut material upon the NARF, three different

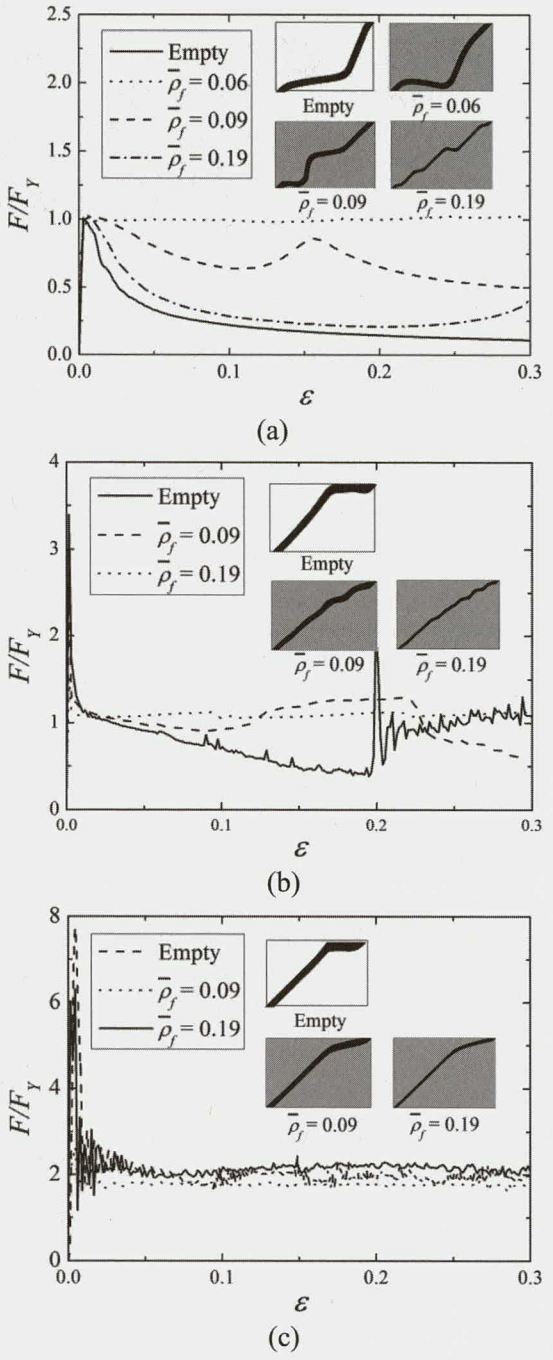

Fig. 8 Influence of foam relative density upon front face reaction force and strut deflection profile of foam-filled panel ($\bar{M} = 0.05$): (*a*) $\bar{V} = 0.0083$, (*b*) $\bar{V} = 0.33$, and (*c*) $\bar{V} = 1$

scenarios were considered: (i) the strut exhibited neither strain hardening nor rate sensitivity; (ii) the strut underwent strain hardening but was strain rate insensitive; and (iii) the strut exhibited both strain hardening and rate sensitivity. The FE simulated results of $\bar{F}$ on both the front and back faces were presented in Fig. 9, with intermediate strut slenderness and foam relative density $L/a = 40$ and $\bar{\rho}_f = 0.13$. When strain hardening was considered, the normalized compression velocity also changed due to change in the plastic wave speed of the strut. Consequently, the compression velocity was normalized below by $\bar{V} = V/(c_{pl} \sin\omega)$ where $c_{pl} = \sqrt{\bar{E}_t/\rho_s}$.

Within the compression velocity range considered, the NARF on the front face was notably enhanced by strut strain hardening. However, in the case of NARF on the back face, the influence of

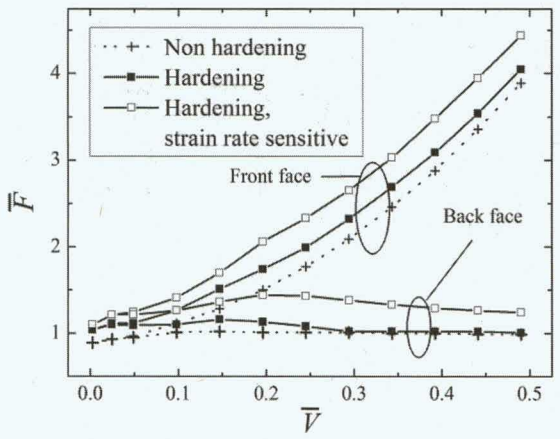

Fig. 9 Influence of strain hardening and strain rate sensitivity of strut material on NARFs for selected compression velocities, with $L/a = 40$ and $\bar{\rho}_f = 0.13$

strut strain hardening seemed to vanish when $\bar{V} > 0.3$. This may be explained as follows. Note first that in the present study the foam-filled corrugated panel was compressed up to $\varepsilon = 0.3$. The time when the nominal compressive strain reached 0.3 (thus the interval for the NARF) was $t = 0.3L\sin\omega/V$, the time it took the propagating plastic wave to reach the back face could be assumed as $t_{\text{pl}} = L/c_{\text{pl}}$. When $\bar{V} = V/(c_{\text{pl}}\sin\omega) > 0.3$, the plastic wave was yet to reach the back face (i.e., $t_{\text{pl}} > t_{0.3}$) and hence the reaction force on the back face remained at the yield level.

In addition to strain hardening, the results of Fig. 9 also demonstrated that the rate sensitivity of the strut material led to increased NARF on both front and back face sheets.

5 Foam/Strut Bonding Condition

When the deformation was sufficiently large, debonding between the filling foam and the strut or face sheets may occur. The influence of debonding was assessed by modeling the corresponding interfaces using hard frictionless contact rather than perfect bonding ("tied" in ABAQUS notation) as employed in Secs. 3 and 4. The two cases may be taken as lower and upper bounds for face sheet reaction forces, provided that foam failure was not considered. Strain rate sensitivity was considered in this section.

For both the front and back face sheets, Figs. 6(*a*) and 6(*b*) compared the NARF $\bar{F}$ calculated using hard frictionless contact with that assuming perfect bonding. It was seen that, when perfect bonding was replaced by hard frictionless contact, the dependency of $\bar{F}$ upon the compression velocity $\bar{V}$ changed little. However, the magnitude of $\bar{F}$ dropped more significantly for panels with higher foam relative density compared to that with lower foam relative density.

6 Dynamic Enhancement

To quantify the strength enhancement of the foam-filled panel by inertia effect and/or constraint provided by foam insertions under different compression velocities, a dynamic enhancement ratio $\bar{F}/\bar{F}_0$ was introduced, equaling to the average reaction force under a particular compression velocity $\bar{V}$ over that under quasi-static compression ($\bar{V} = 0$). Figure 10(*a*) plotted $\bar{F}/\bar{F}_0$ as a function of foam relative density for the full range of compression velocity. Neither strain hardening nor rate sensitivity was considered, and the constraint of same total mass was not enforced. For $\bar{V} \geq 0.5$, the predictions of Eq. (7) were employed for the plotting.

It was seen from Fig. 10(*a*) that, for an empty corrugated panel ($\bar{\rho}_f = 0$), the dynamic enhancement due to inertial effect became significant as the compression velocity was increased. However, at a given compression velocity, inserting foam into the

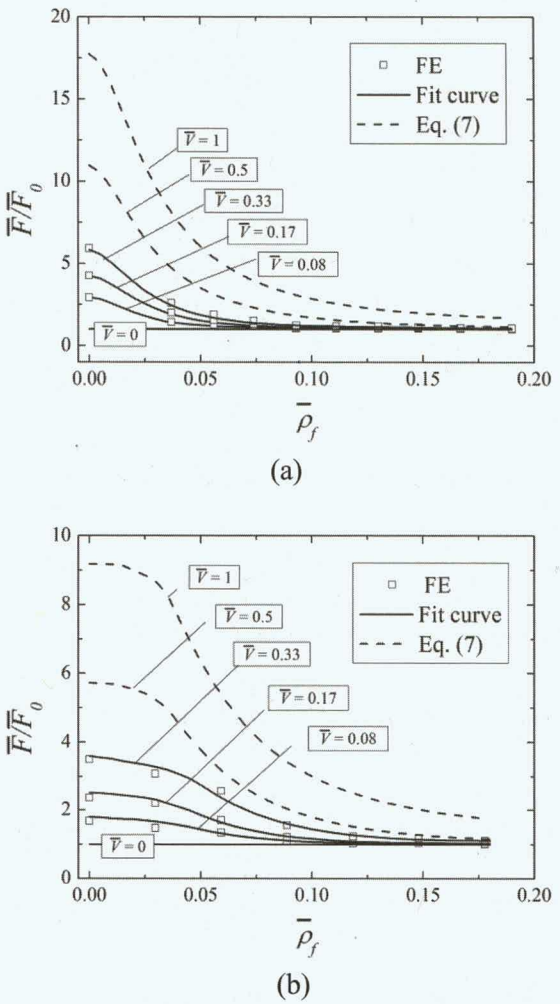

Fig. 10 Dependency of dynamic enhance ratio on foam relative density at selected compression velocities: (*a*) nonhardening and rate insensitive strut, $L/a = 40$, total mass not constrained and (*b*) nonhardening and rate insensitive strut, total mass constrained, $\bar{M} = 0.05$

corrugated core led to reduced dynamic enhancement ratio. This suggested that the constraint of foam filling against strut buckling played an increasingly more important role relative to inertia effect as the compression velocity was increased. For relatively low foam relative densities, the dynamic enhancement was significant because the foam-filled panel behaved like an empty panel, exhibiting low post buckling strength.

As the foam relative density became sufficiently large (e.g., $\bar{\rho}_f > 0.15$), the dynamic enhancement ratio converged to 1 for all compression velocities. This suggested that the increased volume of foam imposed severe constraint in the motion of the strut and the inertia effect did not cause notable enhancement. Consequently, the response was mostly due to the deformation of the foam which remained nearly constant with velocity. This trend continued all the way to higher velocities.

When the total mass was fixed at $\bar{M} = 0.05$, the dependency of dynamic enhance ratio on foam relative density was plotted in Fig. 10(*b*) for selected compression velocities. Relative to the case where the total mass was not constrained (Fig. 10(*a*)), the dynamic enhancement ratio became smaller, which may be reasoned as follows. An empty panel with $\bar{M} = 0.05$ had a strut aspect ratio of $L/a = 20$ considerably stockier than that in the empty panel of Fig. 10(*a*) which had $L/a = 40$. Therefore, the former was more resistant to buckling under quasi-static compression. As the compression velocity was increased, the strut was stabilized by inertia

for both $L/a = 20$ and $L/a = 40$ so that the panel having slender struts exhibited more significant dynamic enhancement. The above reasoning holds for panels filled with relatively low density foams. Otherwise, no notable difference was observed between Figs. 10(*a*) and 10(*b*): the dynamic enhancement ratio decreased with increasing foam relative density and converged to 1 as the relative density approached the limit. Similar results were obtained when strain hardening and rate sensitivity were both considered.

7 Conclusion

The dynamic compressive response of aluminum foam-filled metallic corrugated panels has been investigated systematically using the method of FEs. The following conclusions were obtained:

(a) Three collapse modes were identified: quasi-static mode, transition mode and shock mode, corresponding to different ranges of compression velocity.
(b) At low compression velocities, the foam-filled panel was more efficient in energy absorption compared to the empty panel due to the lateral support provided by the filling foam against strut buckling if the foam relative density was sufficiently large. The benefit of foam filling persisted if the constraint of same total mass was enforced. When the foam density was relatively small, there is no advantage to filling the core with foam for structural purposes.
(c) At transitional compression velocities, the influence of inertial stabilization upon strut buckling was no longer negligible especially when the foam relative density was relatively small.
(d) At sufficiently high compression velocities, the foam-filled panel exhibited a shock-wave-like response that could be analytically described by applying the conservation of momentum.
(e) The bonding condition between the foam insertions and the strut or face sheets had notable influence on the dynamic crushing response of the foam-filled panel. Modeling the interfaces by hard frictionless contact rather than perfect bonding reduced the average reaction forces on both the front and back face sheets.
(f) The strength enhancement caused by inertia effect was most significant for empty panel and foam-filled panel having relatively low foam densities. When the foam density exceeded a certain limit, the increased volume of foam imposed severe constraint in the motion of the strut. Consequently, the response was mostly due to the deformation of the foam which remained nearly constant with velocity. This trend continued all the way to higher velocities.

With high specific strength and specific energy absorption, all-metallic sandwich panels filled with aluminum foams hold great potential as novel lightweight structural materials for a wide range of applications. Recent studies showed that the mechanical properties of metal fiber networks, when compared with metal foams, are also very promising [12–14]. Future studies will be devoted to quantify the static and dynamic energy absorption capacity of sandwich panels with metal fiber networks as the core.

Acknowledgment

This work was supported by the National Basic Research Program of China (2011CB610305), the National Natural Science Foundation of China (11021202, 11072188 and 11102152), the National 111 Project of China (B06024), and the Fundamental Research Funds for Xi'an Jiaotong University (xjj2011007).

Reference

[1] Calladine, C. R., and English, R. W., 1984, "Strain-Rate and Inertia Effects in the Collapse of Two Types of Energy-Absorbing Structure," Int. J. Mech. Sci., **26**(11–12), pp. 689–701.
[2] Yan, L. L., Yu, B., Han, B., Chen, C. Q., Zhang, Q. C., and Lu, T. J., 2013, "Compressive Strength and Energy Absorption of Sandwich Panels With Aluminum Foam-Filled Corrugated Cores," Compos. Sci. Technol., **86**, pp. 142–148.
[3] Han, B., Yan, L. L., Yu, B., Chen, C. Q., Zhang, Q. C., and Lu, T. J., 2014, "Collapse Mechanism Maps for Metal Sandwich Plates With Aluminum Foam-Filled Corrugated Cores," J. Mech. Mater. Strut., **9**(4), pp. 397–425.
[4] Vaziri, A., Xue, Z., and Hutchinson, J. W., 2006, "Metal Sandwich Plates With Polymer Foam-Filled Cores," J. Mech. Mater. Struct., **1**(1), pp. 97–127.
[5] Stout, M. G., and Follansbee, P. S., 1986, "Strain Rate Sensitivity, Strain Hardening, and Yield Behavior of 304L Stainless Steel," ASME J. Eng. Mater. Technol., **108**(4), pp. 344–353.
[6] Deshpande, V. S., and Fleck, N. A., 2000, "Isotropic Constitutive Models for Metallic Foams," J. Mech. Phys. Solids, **48**(6–7), pp. 1253–1283.
[7] Hanssen, A. G., Hopperstad, O. S., Langseth, M., and Ilstad, H., 2002, "Validation of Constitutive Models Applicable to Aluminium Foams," Int. J. Mech. Sci., **44**(2), pp. 359–406.
[8] Gibson, L. J., and Ashby, M. F., 1997, *Cellular Solids: Structure and Properties*, Cambridge University Press, Cambridge, UK.
[9] Pattofatto, S., Elnasri, I., Zhao, H., Tsitsiris, H., Hild, F., and Girard, Y., 2007, "Shock Enhancement of Cellular Structures Under Impact Loading: Part II Analysis," J. Mech. Phys. Solids, **55**(12), pp. 2672–2686.
[10] Mcshane, G. J., Pingle, S. M., Deshpande, V. S., and Fleck, N. A., 2012, "Dynamic Buckling of an Inclined Strut," Int. J. Solids Struct., **49**(19–20), pp. 2830–2838.
[11] Vaughn, D. G., Canning, J. M., and Hutchinson, J. W., 2005, "Coupled Plastic Wave Propagation and Column Buckling," ASME J. Appl. Mech., **72**(1), pp. 139–146.
[12] Markaki, A. E., and Clyne, T. W., 2003, "Mechanics of Thin Ultra-Light Stainless Steel Sandwich Sheet Material," Acta Mater., **51**(5), pp. 1341–1350.
[13] Jin, M. Z., Chen, C. Q., and Lu, T. J., 2013, "The Mechanical Behavior of Porous Metal Fiber Sintered Sheets," J. Mech. Phys. Solids, **61**(1), pp. 161–174.
[14] Jin, M. Z., Zhao, T. F., and Chen, C. Q., 2014, "The Effects of Micro-Defects and Crack on the Mechanical Properties of Metal Fiber Sintered Sheets," Int. J. Solids Struct., **51**(10), pp. 1946–1953.